Wave-Skewness And Current-Related Ebb-Tidal Sediment Transport: Observations And Modeling

Reniers, Ad; de Wit, Floris; Tissier, Marion; Pearson, Stuart; Brakenhof, L.B.; van der Vegt, M.; Mol, J.; van Prooijen, Bram

DOI
10.1142/9789811204487_0174

Publication date
2019

Document Version
Final published version

Published in
Coastal Sediments 2019

WAVE-SKEWNESS AND CURRENT-RELATED EBB-TIDAL SEDIMENT TRANSPORT: OBSERVATIONS AND MODELING

A.J.H.M. RENIERS[1], F.P. DE WIT[1], M.F.S. TISSIER[1], S.G. PEARSON[1,2], L.B. BRAKENHOFF[3], M. VAN DER VEGT[3] , J. MOL[4], B.C. VAN PROOIJEN[1]

1. *Department of Hydraulic Engineering, Delft University of Technology, Delft, the Netherlands.* a.j.h.m.reniers@tudelft.nl, s.g.pearson@tudelft.nl, b.c.vanprooijen@tudelft.nl, f.p.dewit@tudelft.nl, m.f.s.tissier@tudelft.nl
2. *Deltares, Delft, the Netherlands.*
3. *University of Utrecht, Utrecht, the Netherlands.* l.b.brakenhoff@uu.nl, m.vandervegt@uu.nl
4. *Rijkswaterstaat, Ministry of Infrastructure and Water Management, the Netherlands.* janwillem.mol@rws.nl

Abstract: A combination of observations and modeling of wave-and current-related sediment transport at the ebb-tidal delta of Ameland, The Netherlands, has been used to examine the dominant sediment transport contributions shaping the ebb-tidal delta. The calibrated model shows a good comparison with the observations for a range of conditions. The results show distinctly different transport modes and directions for current and wave-dominated conditions respectively, with a significant contribution owing to the skewness of the waves emphasizing the importance of wave non-linearity in shaping the ebb-tidal delta.

Introduction

Ebb-tidal deltas have an important function in coastal safety as they dissipate incident wave energy during storm conditions. Furthermore, they act as a buffer of sediment feeding the adjacent coasts. In the Wadden Sea there has been a gradual decay of the ebb-tidal sediment volumes due to an influx of sediment into the Wadden Sea (left panel Fig. 1). Part of this influx is related to the closure of the Zuiderzee in 1932 creating Lake IJssel, with a Wadden Sea bathymetry that is overall too deep for the reduced tidal prism, leading to a need for sediment. This is exacerbated by the concurrent sea level rise (SLR) and is thus expected to continue in the foreseeable future, thereby increasingly exposing the adjacent barrier islands to storm impacts. To mitigate these storm impacts the current approach is to use local small-scale shoreface nourishments to keep the barrier island shorelines in place. Alternatively, large ebb-tidal delta nourishments could be used to meet multiple goals, i.e. the influx of sediment into the Wadden Sea to keep up with the SLR as well as feeding the adjacent coasts and creation of favorable ecological habitats. To design effective nourishments, the sediment exchange of the ebb-tidal delta in the presence of

waves and currents needs to be better understood. A key factor in this is the interaction between waves and currents. This interaction occurs 1) at the wave-averaged scale, where the stirring of sediment by wave orbital velocities can lead to a preferential current-related sediment transport direction depending on the differences in wave-attenuation for opposing and following flows and 2) the attenuation may affect the near-bed velocity skewness, thus affecting also the wave-related sediment transport. To explore the wave-current effects on the sediment transport processes a large-scale field experiment has been performed in the summer of 2017 at the Ameland inlet (lower panels of Fig. 1) with specific attention for the intra-wave skewness-related sediment transport.

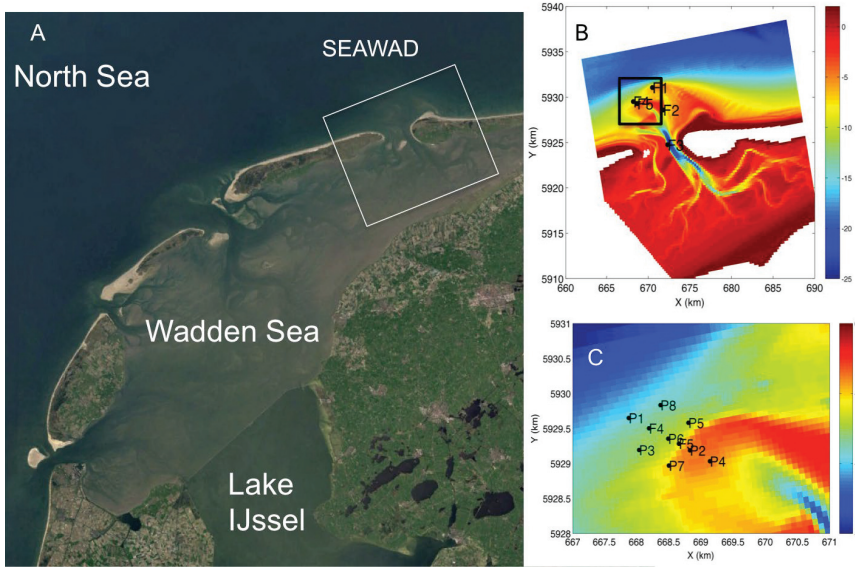

Fig. 1. Panel A: Location of SEAWAD field site in the Netherlands. Panel B: Ameland inlet with instrument locations on the ebb-tidal delta (white box in panel A). Panel C: Position of instrument frames 4 and 5 and pressure sensors 1-8 at the distal end of the ebb-channel (black box in panel B).

Methodology

Two instrument frames equipped with ADVs, up-and downward looking ADCPs, OBS and pressure sensors were deployed at the distal end of the westerly ebb-tidal channel (lower left panel Fig. 1). This was complemented with an array of pressure sensors (lower right panel of Fig. 1), as well as GPS-equipped drifter measurements, to examine the wave and current dynamics and associated sediment transport. The deployment allows for a temporal and spatial analysis of the hydro- and sediment dynamics. These observations are combined

with numerical modeling using the Delft3D modeling suite to connect the local observations to the regional processes related to the tidal exchange between the North Sea and Wadden Sea through the Ameland inlet. The model is driven by tidal hydrodynamic boundary conditions and offshore wave conditions. Model predictions are verified with the local observations of the wave conditions and tidal flow velocities prior to computing the concurrent sediment concentrations and transports. By considering multiple tidal cycles the dominant transport mechanisms as function of the interaction between waves and currents will be established, both for the wave-averaged current transport and the wave-related contributions associated with wave skewness.

Wave conditions are obtained from an offshore wave buoy and imposed as boundary conditions at both the lateral and offshore boundaries of the model domain (middle panel of Fig. 1). The wave modeling is performed with SWAN (Booij *et al.*, 1999) including refraction, shoaling, depth-induced wave breaking, wave-current interaction, wind forcing, white capping, quadruplets and bed friction. Flow computations are perfomed in depth-averaged mode including the effects of bed friction, wind and wave forcing as well as horizontal mixing (Lesser *et al.*, 2004). The bed-shear stress is a combination of the current related stress using a Manning coefficient of 0.024 and the wave related stress according to Fredsoe (1984) using the parameterization of Soulsby *et al.* (1997). The tidal boundary conditions are obtained from the European Shelf model (Egbert *et al.*, 2010), with some local amplitude corrections based on the observations. The wind induced surge levels associated with the storms are superimposed on the tidal boundary conditions using Riemann time series. The lateral wind-induced currents are obtained from a simplified alongshore momentum balance assuming that the tidally averaged wind stress and bed-friction are in balance (Colossimo *et al.*, 2019) and added to the Riemann boundary conditions. The sediment transport is computed using van Rijn's formulations (van Rijn, 1993; van Rijn, 2000) describing both suspended and bed-load sediment transports including wave skewness contributions using the method of Isobe and Horikawa (1982).

Results

Wave and flow conditions are varying throughout the field experiment with wave heights up to 5 m (panel a of Fig. 2), predominantly arriving from the south-west to north-westerly directions (panel c) generated by local winds (panel e) resulting in relatively short period waves (panel b). The tidal elevation is diurnual with elevated surge levels during storm conditions (compare panels a and d in Fig. 2). To examine the combined effect of the waves and currents on

the ebb-tidal delta sediment transport a three day period near the end of the field experiment is considered starting on yearday 274 (see Fig. 2).

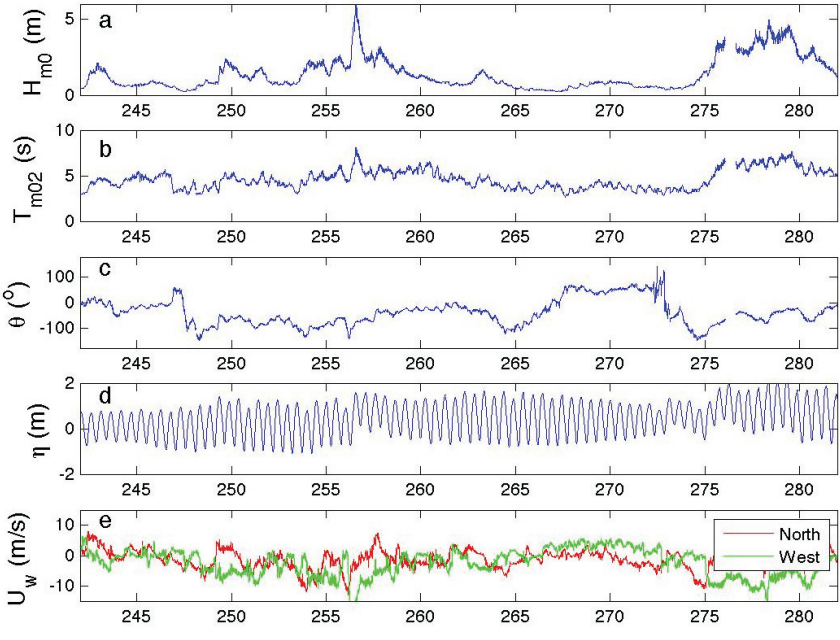

Fig. 2. Panel a: Measured offshore significant wave height as function of yearday. Panel b: Measured offshore mean wave period. Panel c: Measured offshore mean wave direction (nautical convention). Panel d: Observed tidal and surge elevation at P1. Panel e: Observed wind velocities (positive to the East and North respectively).

A snapshot of the computed wave height for yearday 276 at 0.0 hours shows significant spatial variability reflecting the undulations in the bathymetry (Fig. 3). At this time offshore wave heights are in the order of 2.5 m incident from the North-West (Fig. 2) and thus more or less aligned with the array transect direction. The tide is outgoing resulting in offshore directed lagrangian transport pathways obtained by time-integrating the wave-averaged velocities for 30 minutes (left panel of Fig. 3).

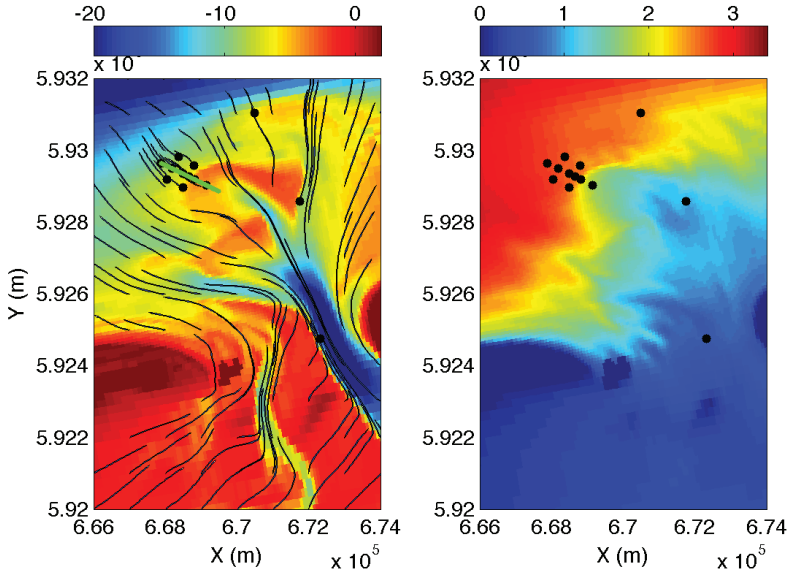

Fig. 3. Model predictions obtained for yearday 276 at 0.0 hours. Left panel: Lagrangian arrows super imposed on the bathymetry (bed level with respect to mean sea level in m). Model array transect in green with the instrument locations denoted by the black dots. Right panel: Predicted significant wave height (height in m).

To avoid problems associated with translating the near-bed wave-related pressure to a surface elevation using linear wave theory to estimate the incident wave height in deeper water, instead the model predictions of the wave height are used to compute the equivalent significant pressure wave height at the bed. Comparing the measured and predicted pressure wave height for the three day period shows a fair comparison at the different sensors of the measurement array (Fig. 4). Waves are moslty absent during yearday 274, followed by a rapid increase in the wave height on yearday 275 after which it stays more or less constant during yearday 276. Wave breaking is apparent at sensors in shallower locations showing a tidally modulated wave height (see sensor P4 for example in Fig. 4).

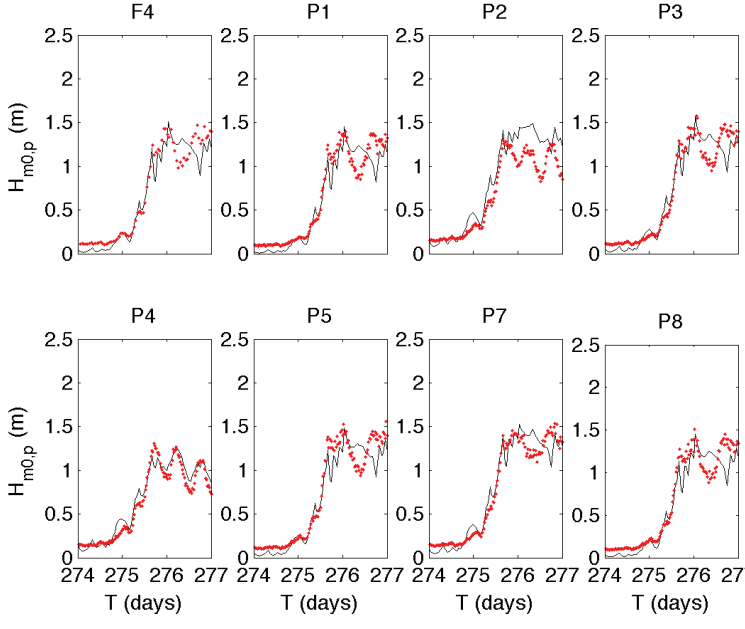

Fig. 4. Computed (solid gray line) and measured (red dots) equivalent significant pressure wave height at the bed for a three day period. Corresponding sensor locations are given in the right panel of Fig. 1.

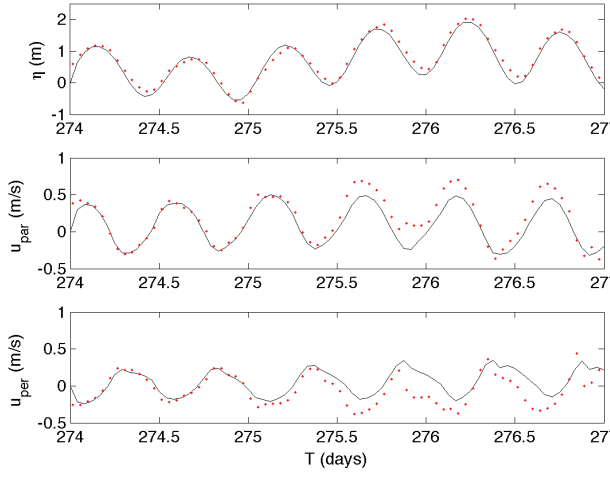

Fig. 5. Top panel: Tidal elevation at sensor location F4. Middle panel: Tidal velocity parallel to the instrument array at F4. Bottom panel: Tidal velocity perpendicular to the instrument array at F4. Measurements are indicated by the red dots, model results by the gray lines.

Next the wave-averaged flow velocities and tidal elevation are verified with observations at F4. Both modeled and observed velocities are decomposed in velocities parallel to the instrument array, u_{par}, being positive towards the inlet mouth, and perpendicular to the array, u_{per}, using the cartesian convention. Model predictions for the tide and surge elevation at F4 correspond well (upper panel of Fig. 5). The wave-averaged velocities compare well during the quiescent conditions of yearday 274 for both parallel and perpendicular velocities. As the wave height increases errors in the predicted velocities occur resulting in un underestimation of the velocity magnitudes during yeardays 275 and 276.

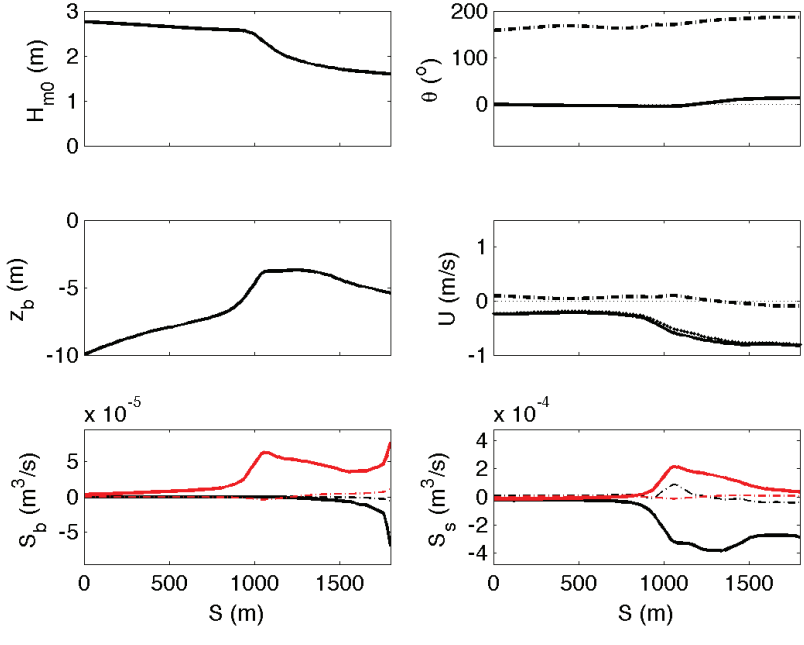

Fig. 6. Model predictions along the array transect for yearday 276 at 0.0 hr. Upper left panel: Significant wave height. Upper right: Wave direction (solid black line) and current angle (dash-dotted line) with respect to the orientation of the array transect. Middle left panel: Bed level. Middle right panel: Parallel velocity (solid black), perpendicular velocity (dash-dotted) and co-linear velocity with the waves (black dots). Lower left panel: Bed load sediment transport by waves (thick red for parallel and thin red line for perpendicular transports) and currents (thick black for parallel and thin black line for perpendicular transports). Lower right panel: The same for the suspended sediment transport (note the **difference** in the vertical scale). Positive transports are into the inlet.

The wave, flow and sediment transport distribution along the array transect are examined next. A snapshot for yearday 276 at 0.0 hrs, corresponding to the

conditions shown in Fig. 2, shows a strong decrease in the wave height (upper left panel of Fig. 6) as the waves propagate on to the ebb tidal shoal (middle left panel of Fig. 6). The wave direction is aligned with the instrument array whereas the flow direction is in the opposite direction (upper right panel of Fig. 6) corresponding to an opposing current for the incident waves (middle right panel). Instantaneous bed-load sediment transport is dominated by the wave-skewness related contribution, whereas the suspended sediment transport is dominated by the offshore directed current related sediment transport. Note that the strirring effect of the waves is incorporated in the current related sediment transport. Given the difference in scaling, compare the two upper panels, the results show a predominantly offshore directed total sediment flux.

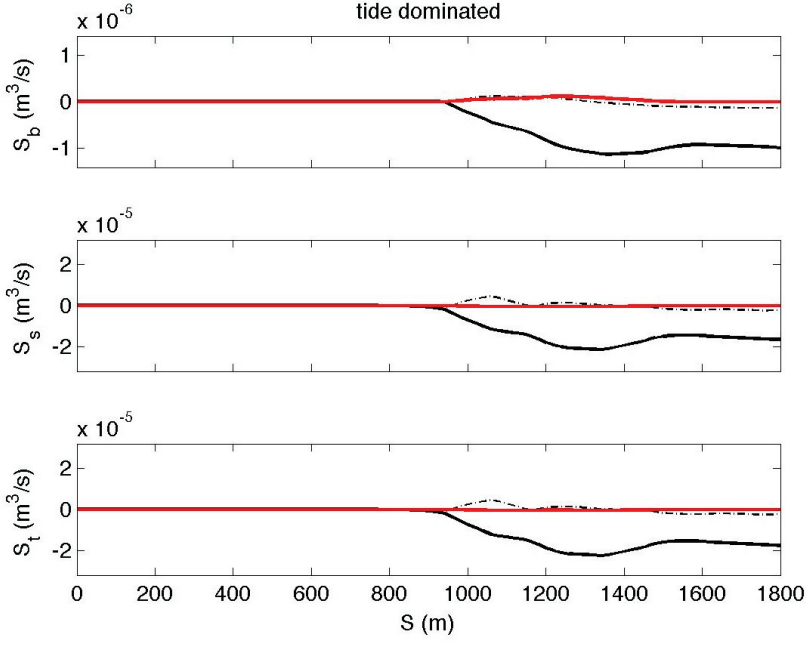

Fig. 7. Upper panel: Daily averaged predicted bed load sediment transport by waves (thick red for parallel and thin dashed red line for perpendicular transports) and currents (thick black for parallel and thin dashed black line for perpendicular transports) for yearday **274**. Middle panel: The same for the suspended sediment transport (note the difference in the vertical scale). Lower panel: Total sediment transport.

To get a more complete picture, the hourly predicted sediment transports are daily-averaged for days 274 and 276 corresponding to tide-dominated and wave-dominated conditions respectively as a proxy for the tide-averaged sediment

transports. The tide-dominated daily-averaged sediment transport shows an offshore flux of sediment associated with the outflow of the tide from the channel in both the bed-load and suspended load (Fig. 7). The transport is mostly parallel to the instrument array with minimal transport perpendicular to the transect resulting in a net flux of sediment out of the inlet.

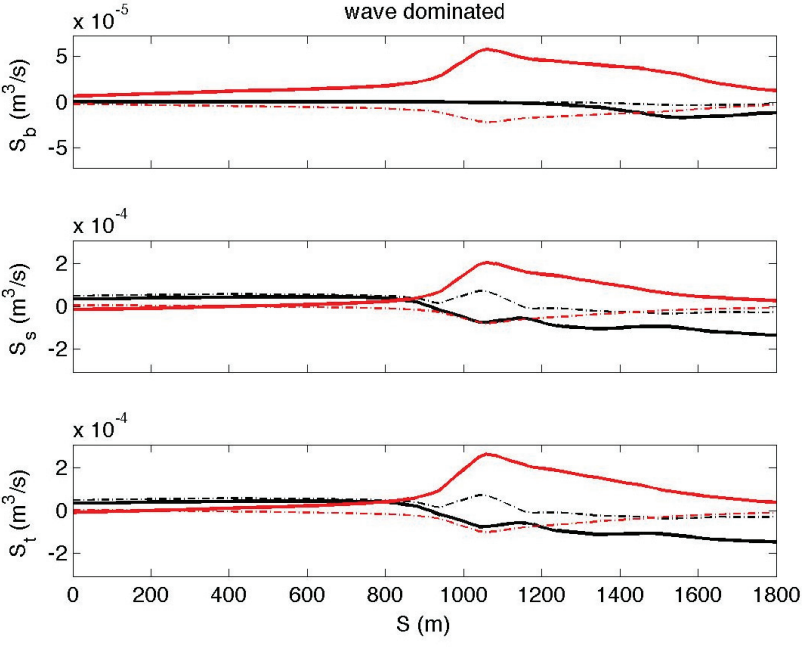

Fig. 8. Upper panel: Daily averaged predicted bed load sediment transport by waves (thick red for parallel and thin red line for perpendicular transports) and currents (thick black for parallel and thin black line for perpendicular transports) for yearday **276**. Middle panel: The same for the suspended sediment transport (note the difference in the vertical scale). Lower panel: Total sediment transport.

Examing the wave-dominated conditions next yields very different results (Fig. 8). Offshore of the ebb-tidal shoal the bed-load sediment transport is dominated by the wave-related transport resulting in an onshore contribution (upper panel of Fig. 8). The wave-related transport increases further with decreasing depth dominating the current-related bed load transport. The daily averaged suspended sediment transport offshore also shows an onshore flux, but in this case due to the current related transport (middle panel of Fig. 8). As the water depth decreases the current related transport switches from being onshore to off-shore directed on the ebb-tidal shoal (middle panel of Fig. 8). At the same time the wave-skewness related sediment transport increases rapidly as the waves

become more effective at mobilizing the bed with transport rates that are exceeding the current related suspended sediment tranpsort, thus resulting in an overall net-onshore sediment flux.

Conclusions

Model preditions match the observations for a range in conditions. In absence of waves the daily averaged total sediment transport is dominated by suspended load directed out of the inlet. In contrast, during storm conditions the daily averaged total transport is dominated by suspended sediment into the inlet owing to the skewness of the waves. As such these results suggest that wave non-linearity plays an important role in the morphodynamic evolution of the ebb-tidal delta.

Acknowledgements

This work is part of the SEAWAD/Kustgenese 2.0 research program (Project #14489), supported by the Dutch Technology Foundation STW, which is part of the Netherlands Organization for Scientific Research (NWO). Special thanks go to the Ministry of Infrastructure and Water Management (Rijkswaterstaat and Rijksrederij) and Deltares for their technical support and collaboration on this project.

References

Booij, N., R.C. is and L.H. Holthuijsen (1999). A third-generation wave model for coastal regions: 1, Model description and validation, *J. Geophys. Res. Oceans*, Vol. 104, 7649–7666.

I. Colosimo, P.L.M. de Vet, D.S. van Maren, A.J.H.M. Reniers, J.C. Winterwerp and B.C. van Prooijen (2019). Wind-induced effects on intertidal flat sediment transport, paper in preparation.

Egbert, G. D., S. Y. Erofeeva, and R. D. Ray (2010). Assimilation of altimetry data for nonlinear shallow-water tides: quarter-diurnal tides of the Northwest European Shelf, *Continental Shelf Research,* 30, 668–679.

Isobe, M. and K. Horikawa (1982). Study on water particle velocities of shoaling and breaking Waves, *Coastal Eng. in Japan*, 25, 109–123.

Fredsoe, J. (1984). Turbulent boundary layer in wave-current interaction, *J. of Hydraulic Eng.*, 110, 1103–1120.

Lesser, G.R., J.A. Roelvink, J.A.T.M. van Kester and G.S. Stelling (2004). Development and Validation of a Three-Dimensional Morphological Model, *J. Coastal Eng*., 51, 883–915.

Soulsby, R. L., L. Hamm, G. Klopman, D. Myrhaug, R. R. Simons and G. P. Thomas (1993). Wave-current interaction within and outside the bottom boundary layer, *J. Coastal Eng.* 21, 41–69.

Van Rijn, L.C. (1993). Principles of Sediment Transport in Rivers, Estuaries and Coastal Seas, Aqua Publications, The Netherlands.

Van Rijn, L. C. (2000). General view on sand transport by currents and waves, Rep. No Z2899.20 Z2099.30-Z2824.30, Delft Hydraulics, Delft, The Netherlands.